

Hear to Segment: Unmixing the Audio to Guide the Semantic Segmentation

Yuhang Ling
Fudan University
Shanghai, China
21210240062@m.fudan.edu.cn

Yuxi Li
Youtu lab, Tencent
Shanghai, China
yukiyxli@tencent.com

Zhenye Gan
Youtu lab, Tencent
Shanghai, China
wingzygan@tencent.com

Jiangning Zhang
Youtu lab, Tencent
Shanghai, China
186368@zju.edu.cn

Mingmin Chi*
Fudan University
Shanghai, China
mmchi@fudan.edu.cn

Yabiao Wang*
Youtu lab, Tencent
Shanghai, China
caseywang@tencent.com

ABSTRACT

In this paper, we focus on a recently proposed novel task called Audio-Visual Segmentation (AVS), where the fine-grained correspondence between audio stream and image pixels is required to be established. However, learning such correspondence faces two key challenges: (1) audio signals inherently exhibit a high degree of information density, as sounds produced by multiple objects are entangled within the same audio stream; (2) the frequency of audio signals from objects with the same category tends to be similar, which hampers the distinction of target object and consequently leads to ambiguous segmentation results. Toward this end, we propose an Audio Unmixing and Semantic Segmentation Network (AUSS), which encourages unmixing complicated audio signals and distinguishing similar sounds. Technically, our AUSS unmixes the audio signals into a set of audio queries, and interacts them with visual features by masked attention mechanisms. To encourage these audio queries to capture distinctive features embedded within the audio, two self-supervised losses are also introduced as additional supervision at both class and mask levels. Extensive experimental results on the AVSBench benchmark show that our AUSS sets a new state-of-the-art in both single-source and multi-source subsets, demonstrating the effectiveness of our AUSS in bridging the gap between audio and vision modalities.

CCS CONCEPTS

• **Computing methodologies** → *Scene understanding*.

KEYWORDS

multi-modal learning, audio-visual segmentation, unmixing

1 INTRODUCTION

Our environment is filled with audio and visual signals, and humans can effortlessly establish their correspondence and comprehend the semantics of these raw signals. For example, we can quickly identify the source of a siren or a bark and locate it. However, this is a challenging task for machines, making audio-visual research a critical area of focus. Recently, a novel task, called Audio-Visual Segmentation (AVS), has been proposed in [49], which consumes an associated image and audio pair, and then segments the sounding

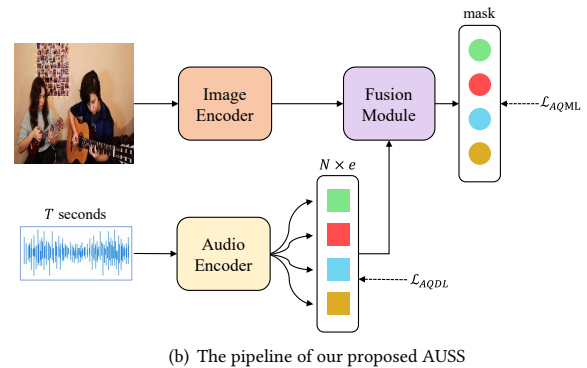
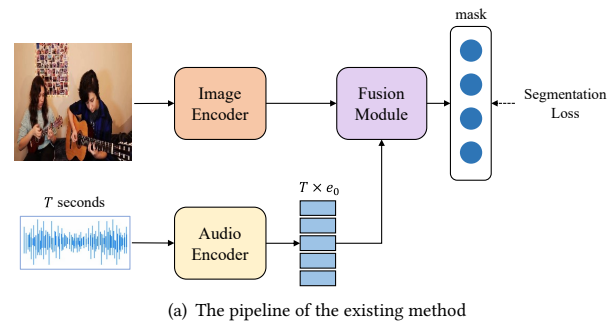


Figure 1: Comparison between existing method [49] and ours. The baseline simply extracts the audio features at each timestamp with an audio encoder while our method unmixes multiple latent components as audio queries and apply 2 designed loss functions, aiming to extract semantic information and increase their heterogeneity.

objects. AVS requires the model to master pixel-level understanding, which is greatly helpful in realizing voice control in complex circumstances.

The AVS is inherently a non-trivial task, owing to the following challenges posed by the intrinsic properties of audio signals. First, the audio signals exhibit a high degree of information density because multiple objects can make sound simultaneously. In a concert scenario, for instance, the sounds of instruments and human voices

*Corresponding authors.

often become intertwined. This phenomenon necessitates the disentanglement of audio signals at each timestamp into multiple latent components to effectively capture the unique sounding features of individual objects. Second, the frequency of audio signals from objects with the same category tends to be similar, such as the Husky and the Tibetan Mastiff (dogs with different breeds). This ambiguity presents greater demands on the audio signal representation throughout the network to avoid inaccurately locating the sources of sound. However, the existing method [49] fails to address these challenges. Specifically, it simply extracts the audio features at each timestamp with an audio encoder, and then interacts with image embedding to generate the final prediction with a mask decoder under the supervision of the standard segmentation loss.

To tackle the aforementioned challenges, we propose a novel framework called Audio Unmixing for Semantic Segmentation (AUSS) to deal with the AVS task. Our AUSS draws inspiration from the remote sensing area, where each pixel in hyper-spectral image consists of multiple components, and the *unmixing* technique [12] is generally adopted to infer and separate these components. Specifically, our AUSS first unmixes the audio stream input into several individual components in the form of learnable audio queries. It is worth mentioning that different audio queries are responsible for capturing distinctive components embedded within this audio stream, which is totally different from the previous method [49] that encodes unified temporal audio representations as shown in the Fig. 1(a). The underlying motivation for such design lies in two aspects. First, as mentioned before, audio query unmixing meets the need of dealing with the complexity of audio sources. Besides, the AVS aims at discovering the existence of sounding objects within the given audio sequence instead of exploring their temporal relations, thus our audio query design is a more compact choice. As shown in the Fig. 1(b), we introduce the Attention-based Audio Unmixing Module (A2U), which captures dependency and consistency between audio signals from different but continuous frames and projects them as audio queries. Although explicitly splitting audio signals in a query manner unmixes components embedded in the audio stream, these queries can not always be optimized to be heterogeneous during the learning process, and their homogeneity can lead to the degeneration of the model. Toward this, we propose two self-supervised loss functions called Audio Query Distance Loss (AQDL) and Audio Query Mask Loss (AQML), which explicitly impose similarity restrictions on audio queries and their decoding masks by pushing audio queries further apart and enforcing mutual exclusivity, respectively. Equipped with A2U, as well as AQDL and AQML, our AUSS sets a new state-of-the-art on AVSBench benchmark across both single-source and multi-source settings.

In summary, our contributions are threefold:

- To avoid redundant information interfering fusion process, we unmix the audio into a set of learnable queries within the proposed attention-based module (A2U).
- We design two self-supervised loss functions, AQDL and AQML, which are of great help in pushing audio queries further apart and enforcing mutual exclusivity, respectively. Both of them are shown effective in generating more precise semantic mask.

- Based on our A2U and loss functions, we propose a novel model called AUSS and conduct quantitative and qualitative experiments on the AVSBench dataset. Results show that AUSS sets a new state-of-the-art result with a significant improvement over the baseline [49]. This demonstrates that our proposed method is promising for bridging the gap between audio signals and pixel-wise understanding.

2 RELATED WORK

2.1 Audio-Visual Learning

To mimic human perception ability, audio-visual learning, aimed at developing computational approaches to learn from both audio and visual modalities, has been a flourishing field in recent years. Researchers have proposed several scenarios to explore and exploit correspondence between audio and visual signals.

Audio-Visual Temporal Correspondence [19] requires models to decide if a given audio sample and video sequence are in sync or out of sync. This task is more challenging than AVC since it necessitates learning relevant temporal-sensitive features for both audio and visual streams to recognize synchronization instead of only semantic correspondence.

Audio-Visual Event Localization [9, 21, 23, 35, 39–42, 50, 51] aims to temporally localize audible or visible events into pre-defined labels. Grounding short and long-range temporal interactions demands effective multi-modal feature correspondence, making this task challenging.

Similarly, Audio-Visual Video Parsing [22, 34, 38, 43] involves parsing a video into temporal event segments and labeling them as either audible, visible, or both. The difficulty mainly lies in that many videos have audible sounds originating outside of the field of view, leaving no visual correspondences, but still contributing to overall understanding.

Despite these advancements, all aforementioned audio-visual tasks remain at the temporal/frame/patch level of understanding. In contrast, Audio-Visual Segmentation (AVS) expects models to predict whether each pixel matches the input audio signal, leading to pixel-level understanding by considering the shape of sounding objects. Furthermore, AVS scenarios contain varying numbers of sound sources, making it even more challenging.

2.2 Semantic Segmentation

Early work in semantic segmentation applied per-pixel Bayesian classifiers based on local image statistics [18]. But for now, the mainstream of semantic segmentation can be divided into two categories: per-pixel classification and mask classification.

Per-pixel classification partitions images into regions of different classes using a classification loss on each pixel. Modern methods focus on fusing long-range context information in the final feature map, such as PPM [46], which applies different kernel sizes to the pooling operator, and [3], which proposes atrous convolutions with varying rates. With the development of powerful transformers [37], recent works like Segmenter [33] and SETR [48] replace traditional convolutional backbones with Vision Transformers (ViT) [8] to capture long-range context information from the first layer by leveraging the advantages of Transformer.

Alternatively, mask classification-based methods predict a set of binary masks, each associated with a single class prediction. This

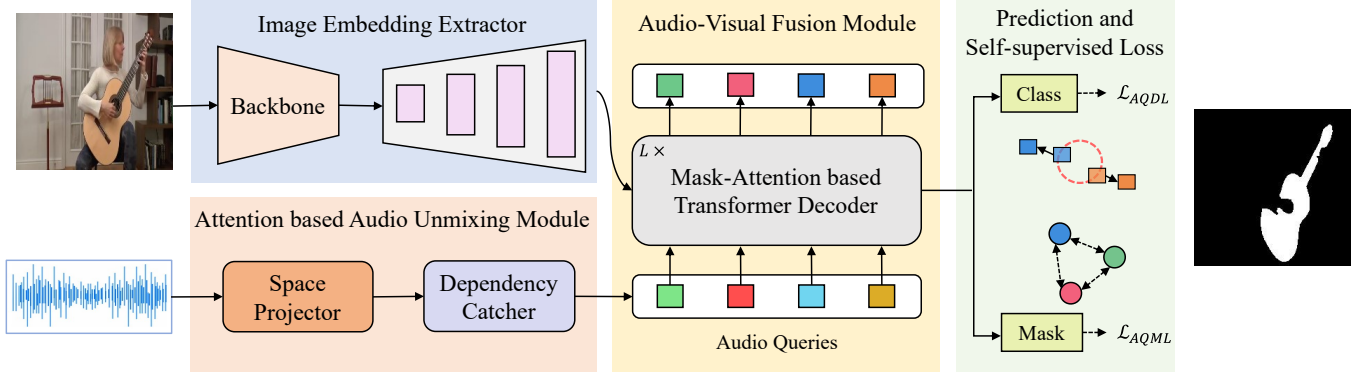


Figure 2: Architecture of Audio Unmixing for Semantic Segmentation (AUSS), which combines hierarchical image features with unmixed audio queries to perform semantic segmentation on images. Comprising three key modules—the Image Embedding Extractor, Attention-based Audio Unmixing Module (A2U), and Audio-Visual Fusion Module—AUSS uses mask attention mechanisms to accurately identify and locate sounding objects within the context of an image. To further enhance its capabilities, we have developed two self-supervised loss functions, \mathcal{L}_{AQDL} and \mathcal{L}_{AQML} , which help to align dense audio queries with relatively sparse image embeddings. Our quantitative experiments have shown these techniques to be highly effective. The square and circle denote audio query and mask, respectively. A mask is generated by the same color query.

flexible method dominated instance segmentation before MaskFormer [6] transferred it to semantic segmentation in a unified manner. Other transformer-based works, such as SegDeformer [32] and k-means MaskFormer [44], were inspired by this approach.

We also notice that several works have focused on multi-modal semantic segmentation, such as TV-Net [16], which is a language-driven semantic image segmentation model capable of segmenting target objects from an image referred to by a given natural language expression. [31] proposed mid-level fusion that allows networks to exploit cross-modal interdependencies between depth images and color information. Notably, SAM [17] was recently proposed to enable networks to understand both sparse (points, boxes, text) prompts and dense (masks) ones. However, audio-visual segmentation occupies little room in this field, and to the best of our knowledge, besides [49], our model is the second to semantically segment image targets with audio signals.

3 METHODOLOGY

In this section, we first present the structure of our proposed network, AUSS, for the pixel-level audio-visual segmentation task. Then, we describe two self-supervised loss functions, Audio Query Distance Loss (AQDL) and Audio Query Mask Loss (AQML), that help to unmix audio and achieve better segmentation results. Finally, we explain how trained AUSS can be used for inference in sec. 3.3.

3.1 Structure of AUSS

As shown in Fig. 2, AUSS takes a sequence of audio and images from a video sequence S , which consists of T non-overlapping but continuous clips $\{S_t^a, S_t^v\}_{t=1}^T$, where S_t^a and S_t^v are the audio and visual components, respectively.

AUSS consists of 3 modules: (1) an attention-based audio unmixing module that transforms audio signals S_t^a into a higher dimensional space and catches dependency and time consistency between

frames, outputs N audio queries $A = \{a_i\}_{i=1}^N$ to guide semantic segmentation; (2) an image embedding extractor, where a backbone extracts image features from S_t^v , followed by gradually upsampling to P multi-scale features $F = \{f_i\}_{i=1}^P$; and (3) an audio-visual fusion module that generates predictions $z = \{z_i | z_i = (a_i, m_i, p_i)\}_{i=1}^N$ by fusing audio queries A with image embeddings F in a mask attention manner, where m_i is the i -th mask, p_i is the probability that m_i corresponds to a sounding object, a_i is the corresponding query.

Attention-based Audio Unmixing Module (A2U): We preprocess audio features followed with [49]. Specifically, given an audio clip S^a , we process it into a spectrogram using short-time Fourier transform, and extract audio features $A_{ori} \in \mathbb{R}^{T \times e_0}$ using VGGish [15], a convolutional neural network pretrained on AudioSet [13].

To unmix dense A_{ori} , we notice that the current embedding space is too narrow to represent the entangled audio signals. To this end, we propose A2U, an attention mechanism-based audio unmixing module, to firstly transform A_{ori} into a higher-dimensional feature space by the Space Projector, and then capture dependency and consistency between frames by the Dependency Catcher. This process projects audio features into a sparse dimensional space while maintain their correlation.

To be specific, the Space Projector is responsible for expanding A_{ori} in both number dimension and channel dimension so as to inject more audio information. Space Projector includes a number projector $W_1 \in \mathbb{R}^{N \times T}$ and a channel projector $W_2 \in \mathbb{R}^{e_0 \times e}$:

$$\hat{A} = W_1 A_{ori} W_2 \quad (1)$$

where $\hat{A} \in \mathbb{R}^{N \times e}$ and $e = 2e_0$.

Meanwhile, there is a dependency and correlation between audio signals from different frames, which also convey important guidance. As what [37] observed, the Self Attention (SA) operation can capture and evaluate this dependency, motivating us to use $N_a = 6$ vanilla transformer encoders as the Dependency Catcher.

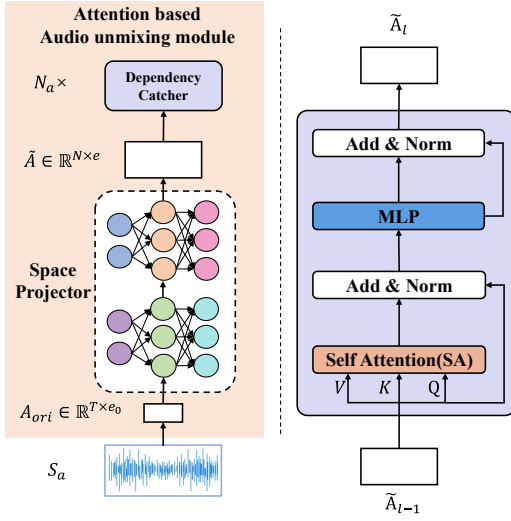


Figure 3: We design a module, called A2U, to unmix dense audio signals, which is consisted of a Space Projector and a Dependency Catcher. The Space Projector expand pre-processed audio features A_{ori} into a higher dimensional feature space in both number and dimension while the Dependency Catcher capture dependency and consistency between audios from frames so as to better unmix them.

Concretely, at l -th layer:

$$\tilde{A}_{SA} = \text{LN}(\text{SA}(Q_l, K_l, V_l) + \tilde{A}_{l-1}) \quad (2)$$

$$\tilde{A}_l = \text{MLP}(\tilde{A}_{SA}) + \tilde{A}_{SA} \quad (3)$$

where LN denotes layer normalization[1] and Q_l , K_l and V_l are linearly transformed from \tilde{A}_{l-1} :

$$Q_l = W_Q(\tilde{A}_{l-1}) \in \mathbb{R}^{N \times e} \quad (4)$$

$$K_l = W_K(\tilde{A}_{l-1}) \in \mathbb{R}^{e \times e} \quad (5)$$

$$V_l = W_V(\tilde{A}_{l-1}) \in \mathbb{R}^{e \times e} \quad (6)$$

$$\text{SA} = \text{softmax}(Q_l K_l^T) V_l \quad (7)$$

specially, \tilde{A} is split into N clips as \tilde{A}_0 . After passing through Space Projector and Dependency Catcher, A2U will output \tilde{A}_6 as audio queries $A = \{a_i\}_{i=1}^N \in \mathbb{R}^{N \times e}$.

Image Embedding Extractor: Receiving $S_t^v \in \mathbb{R}^{H \times W}$ as input, a backbone network generates a low-resolution feature map $f_{ori} \in \mathbb{R}^{C_v \times \frac{H}{d} \times \frac{W}{d}}$, where C_v depends on the specific backbone and $d = 16$ is the stride of the feature map. Then, we gradually upsample the f_{ori} to generate per-pixel embedding set $\tilde{F} = \{f_i\}_{i=1}^{P'}$, where $f_i \in \mathbb{R}^{C_v \times \frac{2^i H}{d} \times \frac{2^i W}{d}}$, and $P' = 4$. We believe that multi-scale image embeddings not only provide necessary context information for understanding circumstance but also reduce the computation cost. We use $F = \{f_i\}_{i=1}^3$ to denote the first three image embedding and keep f_4 for the mask prediction in later.

Audio-Visual Fusion Module: As stated before, A includes audio signal guidance for regions where sound is detected, while F contains abundant visual context information that is essential for

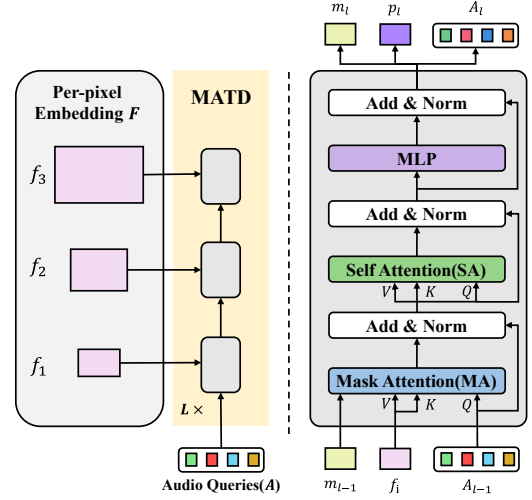


Figure 4: Our Audio-Visual Fusion Module is a collection of L Mask-Attention based Transformer Decoder (MATD) blocks designed to fuse audio queries A with image embeddings F using a round-robin approach. MATD block is capable of using audio signal information from the queries to guide segmentation with context in the image features, helping to create a more comprehensive understanding of the audio-visual content.

image segmentation [3, 4, 47]. However, due to modal heterogeneity, A and F do not align very well. We, as a result, apply mask attention to align them while reducing computation cost as much as possible.

Specifically, our multi-modal fusion module consists of $L = 6$ Mask-Attention based Transformer Decoders (MATD) as depicted in Fig. 4. In the l -th layer, MATD takes audio queries A_{l-1} , attention distribution mask m_{l-1} and image features f_i as input, outputs new audio queries $A_l \in \mathbb{R}^{N \times e}$, attention mask m_l and probability p_l in the two following steps.

First, MATD uses Mask Attention (MA) and Self Attention (SA) to use audio queries A_l to find sounding regions in F :

$$A_{mask} = \text{LN}(\text{MA}(Q_l, K_l, V_l; m_{l-1}) + A_{l-1}) \quad (8)$$

$$A_{self} = \text{LN}(\text{SA}(Q_l, K_l, V_l) + A_{mask}) \quad (9)$$

$$A_l = \text{LN}(g_1(A_{self}) + A_{self}) \quad (10)$$

Then, given the A_l , for probability prediction, MATD will apply a linear classifier, followed by a softmax activation on top of A_l :

$$p_l = \text{softmax}(g_2(\text{LN}(A_l))) \quad (11)$$

where $g_2 \in \mathbb{R}^{N \times K}$ is a linear classifier, $K = 2$ is the number of class.

For mask prediction, a linear transformation g_3 and a 1×1 channel-wise convolution h are used:

$$m_l = \text{sigmoid}(g_3(A_l) \otimes h(f_4)) \quad (12)$$

where $g_3 \in \mathbb{R}^{e \times e}$, $h \in \mathbb{R}^{C_v \times e}$, and \otimes denotes matrix multiplication.

Different from SA, MA additionally introduces a mask attention distribution \tilde{m}_l to reduce training epochs for attending to localized object regions. Concretely, each position (x, y) in \tilde{m}_l follows:

$$\widehat{m}_l(x, y) = \begin{cases} 0 & \text{if } m_l(x, y) > \tau \\ -\infty & \text{in other cases} \end{cases} \quad (13)$$

Empirically, we set $\tau = 0.5$. \widehat{m}_l provides model with information upon local queries in l -layer and fed into $(l+1)$ -layer as mask prediction m_l . f_i in F is projected to K_l and V_l in a round-robin fashion, more details can be found in [5]. Similar to Eq. (7), MA can be formulated as:

$$\text{MA}(Q_l, K_l, V_l; m_{l-1}) = \text{softmax}(m_l + Q_l K_l^T) V_l \quad (14)$$

3.2 Self-Supervised Loss Functions

Though A2U has unmixed embedded components in audio signals as N audio queries, their homogeneity provides ambiguous guidance and consequently leads to a less accurate segmentation. To tackle it, we propose two self-supervised loss functions, Audio Query Distance Loss (AQDL) and Audio Query Mask Loss (AQML), to increase their heterogeneity.

To be specific, AQDL, denoted as \mathcal{L}_{AQDL} , is a penalty on queries that predicts sounding mask but getting too close for each other, indicating that they have a high similarity with less clear guidance. \mathcal{L}_{AQDL} is computed as following:

$$\mathcal{L}_{AQDL} = \frac{2}{n_1(n_1 + 1)} \sum_{i=1}^{n_1} \sum_{j=i+1}^{n_1} d(a_i, a_j) \quad (15)$$

$$d(a_i, a_j) = \begin{cases} \frac{1}{\|a_i - a_j\|_2^2} & \text{if } \|a_i - a_j\|_2^2 < d_0 \\ 0 & \text{in other cases} \end{cases} \quad (16)$$

where a_i and a_j belong to the set $S_1 = \{z_k | p_k > \delta_1\}$, δ_1 is the confidence threshold of \mathcal{L}_{AQDL} , n_1 is the cardinality of S_1 , $\|\cdot\|_2$ is the \mathcal{L}_2 norm, and d_0 is the threshold for $d(a_i, a_j)$.

On the other hand, AQML aims to force queries to predict exclusive sounding mask as much as possible. It calculates how many same pixels are predicted as sound by different audio queries:

$$\mathcal{L}_{AQML} = \frac{2}{n_2(n_2 + 1)} \sum_{i=1}^{n_2} \sum_{j=i+1}^{n_2} I(m_i, m_j) \quad (17)$$

$$I(m_i, m_j) = \frac{1}{2HW} \sum_{x=1}^H \sum_{y=1}^W \text{Bin}(m_i(x, y)) \odot m_j(x, y) + m_i(x, y) \odot \text{Bin}(m_j(x, y)) \quad (18)$$

similar to AQDL, m_i and m_j belong to the set $S_2 = \{z_k | p_k > \delta_2\}$, n_2 is the cardinality of S_2 , and \odot is the Hadamard product.

It is worth noting that how we calculate the intersection of m_i and m_j . A straightforward way is to binarize them and calculate the Hadamard product. However this operation is not derivable due to the binarization. Therefore, we first binarize and detach m_i as pseudo label, calculate Hadamard product and then repeat to m_j . This process is depicted in Eq. (18).

We would like to emphasize that both AQDL and AQML are calculated in self-supervised manner. This property is not only economically benefit but also can generalize well to supervised setting.

Besides AQDL and AQML, we also use some traditional segmentation losses, including focal classification loss \mathcal{L}_{class} [20] and dice

loss \mathcal{L}_{dice} [28], linearly combined as:

$$\mathcal{L} = \lambda_1 \mathcal{L}_{AQDL} + \lambda_2 \mathcal{L}_{AQML} + \lambda_3 \mathcal{L}_{class} + \lambda_4 \mathcal{L}_{dice} \quad (19)$$

3.3 Semantic Inference

After trained with loss in Eq. (19) by backward propagation algorithm, our network AUSS is able to segment all sounding objects in each frame while considering the actual shape of them. In the inference stage, given final output $z = \{z_i | z_i = (a_i, m_i, p_i)\}_{i=1}^N$ at the L -th layer, each pixel (x, y) is predicted via:

$$\arg \max_{c_i} p_i(c_i) * m_i(x, y) \quad (20)$$

$$c_i = \arg \max_{c \in \{1, \dots, K\}} p_i(c) \quad \forall z_i \in z \quad (21)$$

This process assigns a pixel at location (x, y) to i -th mask-probability pair only when both the class probability $p_i(c_i)$ and the mask prediction probability $m_i(x, y)$ are high. All pixels assigned to the same mask-probability pair naturally form a segment whose each pixel is labeled with c_i . In our case, class label = {sound, silent}.

4 EXPERIMENTS

4.1 AVSBench Dataset

We evaluate our proposed method on the AVSBench dataset[49], which is a recently proposed and pixel-level labeled video dataset. It consists of two subsets: single-source videos and multiple-source videos, depending on the number of sounding objects. All videos in the dataset are trimmed to 5 seconds.

The single-source subset contains 4932 videos over 23 categories, covering various sounds, such as humans, animals, vehicles, and musical instruments. Each video in the multiple-source subset includes two or more categories from the single-source subset, and all sounding objects are visible in the frames. The multiple-source subset is consisted of 424 videos. The ratio of train/validation/test split percentages are set as 70/15/15 for both subsets, as shown in Table 1.

Each video in the AVSBench dataset is further divided into five equal 1-second clips, and the last frame of each clip is manually pixel-level annotated. Specially, for videos in the training split of single-source, only the first sampled frame is annotated. During training on the single-source setting, AQDL and AQML provide supervise signal for the network. We follow a *curricular* strategy: first train on the single-source set, then on the multiple-source set. We use the validation set to conduct experimental analysis and compare our method with others on the test set.

Table 1: AVSBench dataset statistics. The 5-second videos are splitted into two subsets. For single-source training split, one annotation per video is provided; all others contain 5 annotations per video.

subset	# of classes	# of videos	train/valid/test	# of annotated frames
single-source	23	4932	3,452/740/740	3452/3700/3700
multiple-source	23	424	296/64/64	1480/320/320

Table 2: Quantitative comparison results of different methods on AVSBench. Our method outperforms Baseline with a great gap. We show that this difference mainly comes from the unmixture of audio signals in A2U and our self-supervised loss functions, i.e., \mathcal{L}_{AQDL} and \mathcal{L}_{AQML} .

Metric	Setting	SSL		VOS		SOD		Baseline[49]		Ours	
		LVS[2]	MSSL[29]	3DC[26]	SST[10]	iGAN[27]	LGVT[45]	ResNet	Pvt-v2	ResNet	Swin-base
$\mathcal{M}_{\mathcal{J}}$	single-source	0.379	0.449	0.571	0.663	0.616	0.749	0.728	0.787	0.831	0.894
	multi-source	0.295	0.261	0.369	0.426	0.429	0.407	0.479	0.540	0.589	0.635
$\mathcal{M}_{\mathcal{F}}$	single-source	0.510	0.663	0.759	0.801	0.778	0.873	0.848	0.879	0.906	0.942
	multi-source	0.310	0.363	0.503	0.572	0.544	0.593	0.593	0.645	0.729	0.752

4.2 Implementation Details

For visual backbone, we choose 2 representative ones: the standard convolution-based ResNet[14] backbone R101 and recently proposed Transformer-based Swin-Transformer[24] backbone swin-base. R101 is pretrained on ImageNet-1K[30] while swin-base on ImageNet-22K.

For the loss weights, we set $\lambda_1 = \lambda_2 = 2.0$ and $\lambda_3 = \lambda_4 = 5.0$. For the optimizer, we use AdamW [25] and the poly [3] learning rate schedule with an initial learning rate of 0.0001 and a weight decay of 0.05 for both R101 and swin-base backbones. A learning rate multiplier of 0.1 is also applied. All models are trained with 8 3090 GPUs for 90k iterations with a batch size of 8.

For data augmentation[7], the standard random horizontal flipping, random cropping, random color jittering as well as random scale jittering between 0.5 and 2.0 are used.

4.3 Main Results

As AVS is a newly proposed problem, we compare our network with baseline in [49] and methods from three related tasks, including sound source localization (SSL), video object segmentation (VOS), and salient object detection (SOD). For each task, we report the results of two SOTA methods on AVSBench dataset, i.e., LVS[49] and MSSL[29] for SSL, 3DC[26] and SST[10] for VOS, iGAN[27] and LGVT[45] for SOD. To ensure fairness, all backbones of these methods were pretrained on the ImageNet dataset.

Quantitative Comparison: Following [49], we use the Jaccard index[11] \mathcal{J} to measure region similarity and F-score \mathcal{F} to evaluate contour accuracy, where $\beta = 0.3$. The quantitative results is shown in Table 2. We use $\mathcal{M}_{\mathcal{J}}$ and $\mathcal{M}_{\mathcal{F}}$ to denote the mean metric values over the whole test dataset. It is evident that there is a significant gap between SSL and our method ($\mathcal{M}_{\mathcal{J}}$: 0.449 vs 0.894), mainly because SSL methods do not consider the actual shape of sounding objects. Besides, our method outperforms Baseline greatly across all backbones. For example, with ResNet as backbone, our model improves by 0.103 $\mathcal{M}_{\mathcal{J}}$ and 0.058 $\mathcal{M}_{\mathcal{F}}$ in the single-source setting. We attribute this improvement to our **audio unmixing** design as well as loss functions: the baseline simply extracts the audio features at each timestamp with an audio encoder, while our model AUSS includes the audio unmixing design that splits audio.

4.4 Ablation Study

We conducted a series of ablation studies to analyze the performance of AUSS. All results are reported on the single-source test split except for specific notation.

Impact of framework: We begin by validating that our improvements are not simply due to the similar framework used in Mask2Former. The primary differences between our approach and Mask2Former are as follows:

- We introduce audio signals and unmix them as audio queries while Mask2Former uses random initialized object queries.
- We use more audio queries to better guide semantic segmentation whereas Mask2Former only has 100 object queries.

As shown in Table 3, directly applying the Mask2Former framework, equipped with swin-base backbone, with randomly initialized object queries resulted in only a small improvement over the baseline, indicating that audio signal input is necessary for effective segmentation. Moreover, even when using audio queries transformed by the number projector from \mathbb{R}^T to \mathbb{R}^N , we observed only a slight improvement in $\mathcal{M}_{\mathcal{J}}$ and $\mathcal{M}_{\mathcal{F}}$, suggesting that valuable audio guidance is present in the input signal and should be leveraged. On the contrary, our model uses A2U, AQDL and AQML to unmix dense audio signals, leading to a significant improvement.

Table 3: Impact of framework. Directly using Mask2Former framework, i.e., without audio input with 100 queries, leads little improvement than baseline. So does more queries.

	# of queries N	$\mathcal{M}_{\mathcal{J}}$	$\mathcal{M}_{\mathcal{F}}$
Baseline: pvt-v2	-	0.787	0.879
w/o audio input	100	0.796	0.883
	200	0.796	0.893
	300	0.798	0.896
w/ audio input	100	0.808	0.893
	200	0.809	0.897
	300	0.809	0.901

Impact of unmixing methods in A2U: In Table 4 we investigate the impact of three different unmixing methods for audio signals in our A2U module. It is easy to conclude that increasing the dimension of the audio queries from 128 to 256 allows them to contain more guidance, and that the attention mechanism is also helpful for unmixing audio queries by learning dependency and semantic consistency among frames and audio context. We would like to emphasize that increasing the number of audio queries, N , does not necessarily result in better performance. When N is less than 300, having more queries is helpful in extracting more audio information. However, when N is larger than 300, both $\mathcal{M}_{\mathcal{J}}$ and $\mathcal{M}_{\mathcal{F}}$ show a decrease. We hypothesize that overlapping audio queries violate our original intention of projecting and sparsely partitioning, resulting in redundant and chaotic fusion processes.

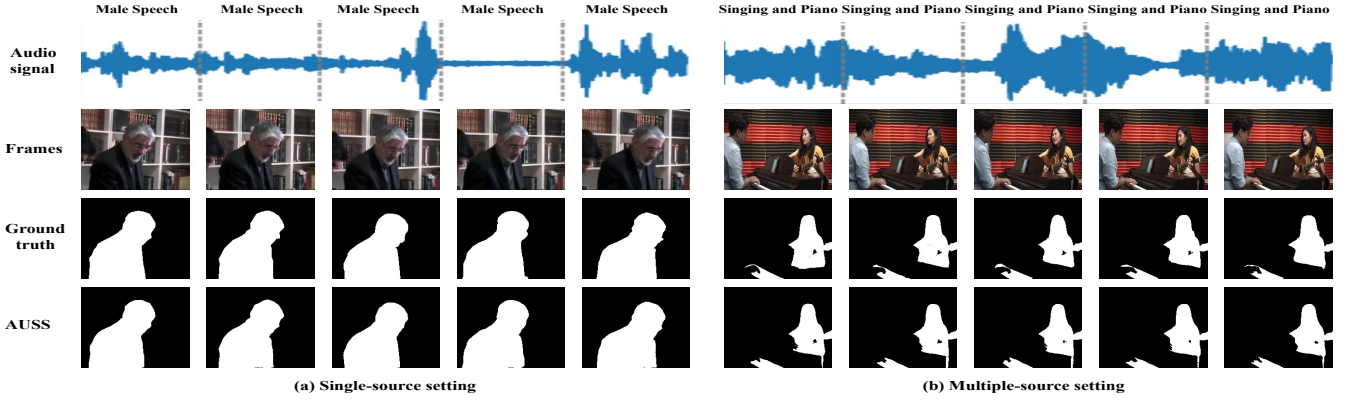


Figure 5: Segmentation on AVSBench in both single-source and multiple-source settings. AUSS can handle semantic segmentation in one or more sound sources circumstance, even though sound sources are moving as right sample shows.

Table 4: Impact of unmixing method of A2U. Increasing the dimension of the audio queries (Dimension projector: $\mathbb{R}^{e_0 \times e}$), using adequate number of audio queries (Number projector: $\mathbb{R}^{T \times N}$) and the attention mechanism (TransformerEncoder: $\mathbb{R}^{N \times N}$) are shown to be effective.

Input size $\mathbb{R}^{T \times e_0}$	Unmix Method			Final size $\mathbb{R}^{N \times e}$	$\mathcal{M}_{\mathcal{J}}$	$\mathcal{M}_{\mathcal{F}}$
	Dimension projector	Number projector	Transformer Encoder			
Baseline:pvt-v2	-	-	-	-	0.787	0.879
5 × 128	✓			5 × 256	0.793	0.872
	✓	✓		100 × 256	0.808	0.874
	✓	✓		300 × 256	0.813	0.877
	✓	✓	✓	300 × 256	0.818	0.895
	✓	✓	✓	500 × 256	0.812	0.894
	✓	✓	✓	700 × 256	0.806	0.894

Impact of proposed module and loss functions: Table 5 demonstrates that our proposed A2U module and self-supervised loss functions contribute to the overall improvement of our model. Furthermore, we compare 2 mode of confidence threshold δ in loss functions, (1) fixed mode: $\delta_1 = \delta_2 = 0.6$; and (2) increasing mode:

$$\delta_i = 0.55 + \frac{0.1}{17} \times \left\lfloor \frac{\text{iterations}}{5000} \right\rfloor, i \in \{1, 2\} \quad (22)$$

Results show that increasing mode yields better results than using a fixed threshold. We hypothesize that this phenomenon can be explained as follows: as AUSS becomes increasingly confident about its mask prediction, a fixed threshold may not penalize audio queries with less confidence at earlier stages, while pushing too many audio queries away at later epochs. This results in poorer performance compared to using an increasing threshold.

Impact of pretrained on single-source subset: As introduced in section 4.1, the videos in the multiple-source subset share similar categories to those in the single-source subset. A natural idea is whether we can pretrain the model on the single-source subset to help deal with the multiple-source problem. As shown in Table 6, we test two initialization strategies, i.e., from scratch or pretrained

Table 5: Impact of A2U Module, \mathcal{L}_{AQDL} and \mathcal{L}_{AQML} . All our proposed modules and loss functions are found to contribute to the final model.

	$\mathcal{M}_{\mathcal{J}}$	$\mathcal{M}_{\mathcal{F}}$
Baseline: ResNet	0.728	0.848
A2U only	0.818	0.895
\mathcal{L}_{AQDL} with increasing δ_1	0.813	0.895
\mathcal{L}_{AQDL} with fixed $\delta_1 = 0.6$	0.804	0.894
\mathcal{L}_{AQML} with increasing δ_2	0.807	0.881
\mathcal{L}_{AQML} with fixed $\delta_2 = 0.6$	0.805	0.877
Ours: ResNet	0.831	0.906

on the single-source subset. It is evident that pretraining on single-source split is beneficial in all the settings. Directly learning on the multiple-source set is too hard to learn, leading a close or worse metric in $\mathcal{M}_{\mathcal{J}}$ and $\mathcal{M}_{\mathcal{F}}$, which proves that our curricular training strategy is beneficial.

Table 6: Impact of pretrained on single-source subset. Results across all backbones show that our curricular training strategy is beneficial.

	$\mathcal{M}_{\mathcal{J}}$		$\mathcal{M}_{\mathcal{F}}$	
	R101	swin-base	R101	swin-base
Baseline	0.479	0.540	0.593	0.645
From scratch	0.408	0.534	0.610	0.674
Pretrained on single-source	0.589	0.635	0.729	0.752

4.5 Visualization

Segmentation result of AUSS: First, we show some segmentation samples on AVSBench in both single-source and multiple-source settings. As Figure 5 shows, AUSS can segment sounding objects

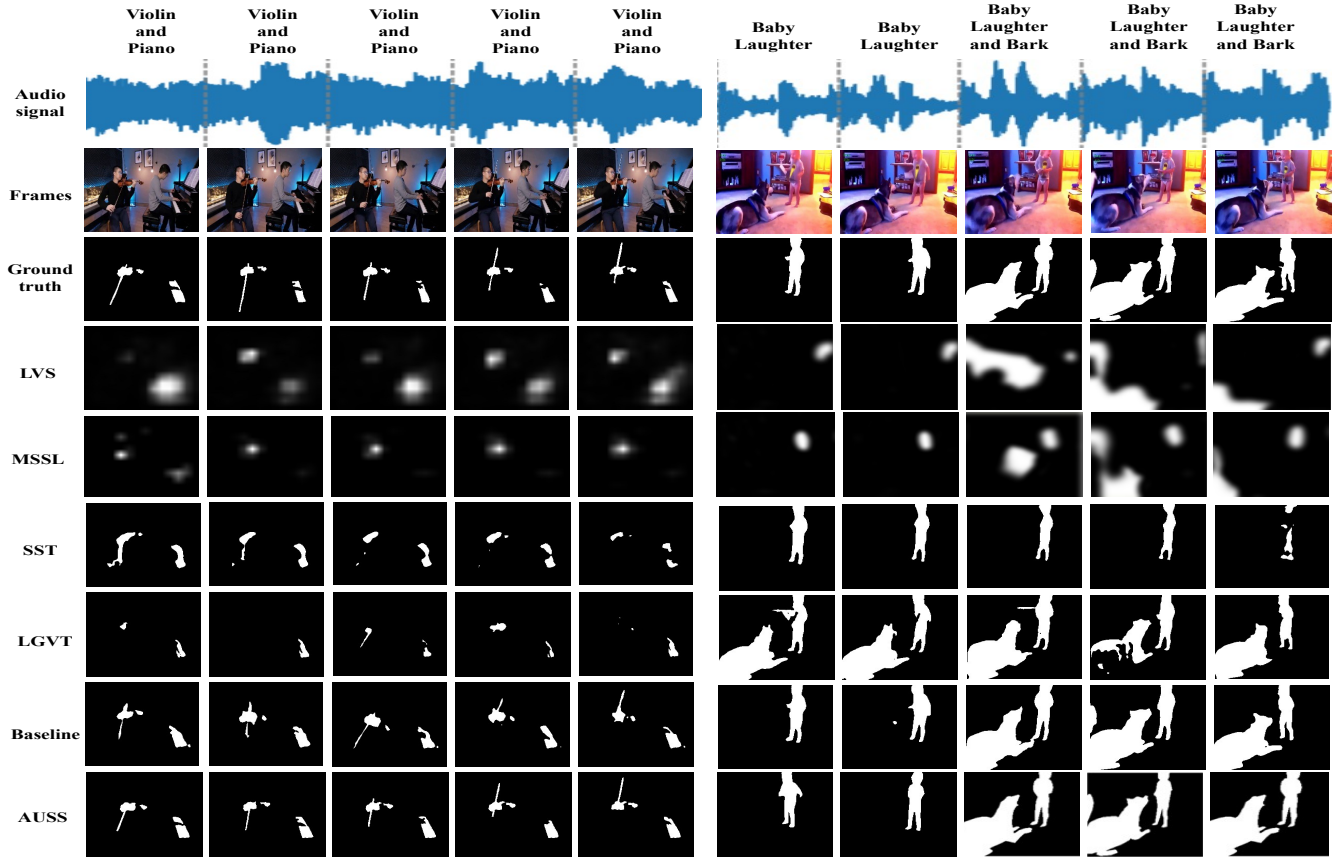


Figure 6: Qualitative comparison between different methods. LVS and MSSL are too blurry and locate coarsely, while SST and LGVT rely on data prior and fail to filter silent object. Both the baseline and our AUSS model can adaptively segment sounding objects but AUSS can delineate the actual shape with a more fine-grained manner.

in one or more sound sources circumstance. Specially, as the right sample of Figure 5 shows, even though the 2 sound sources, woman and piano, are from different categories and far from each other, AUSS can still localize and segment them with a satisfying result.

Qualitative comparison between different methods: the left sample of Figure 6 shows that LVS overlocates the violin while MSSL fails to locate it. Both methods produce blurry outputs. In the first 2 frames of the right sample, SST ignores the dog and only detects the child as a sound source, while LGVT regards the silent dog as a sound source. Both the baseline and AUSS model can segment sounding objects adaptively, but AUSS can delineate the actual shape more finely, such as the small violin bow in the left sample and the baby’s gesture in the right sample.

T-SNE[36] for unmixing visualization: We also visualize the audio queries before and after the audio-fusion module, to show how dense the audio queries are before fusion and how our module unmix them. Specifically, on the test split of the multi-source set, we use the swin-base based AUSS model to obtain audio queries. Since the multi-source set do not have category labels (its videos may contain several categories), we first use the principal component analysis (PCA) to divide the audio queries into $K_0 = 20$ clusters. Then we assign the audio cluster labels to the corresponding audio

queries. In this case, if A_6 is the unmixing result of dense A_0 , then audio queries from the same cluster should get far away from each other while maintaining some similarity. We use the t-SNE visualization to verify this assumption. As shown in Figure 7, more points are depicted after fusion (320 vs 60), and audio queries sharing the same color consists of more different but closely connect clusters, indicating that audio information in A_0 is so dense that most of them are too close to show differences while the unmixing process makes the audio queries more informative and easier to leverage.

5 CONCLUSION

In this paper, we focus on the pixel-wise audio-visual segmentation problem and propose a model called AUSS, which unmixes dense audio signals as audio queries and fuses them with image embeddings by mask attention mechanism. We also propose two loss functions to further unmix audio queries from distance and mask perspectives in a self-supervised manner. We conduct numerous quantitative and qualitative experiments on the AVSBench dataset in both single-source and multiple-source settings. The quantitative results show that our model achieves state-of-the-art performance across all backbones, and the qualitative figures demonstrate that our unmixing approach performs effectively. These results indicate

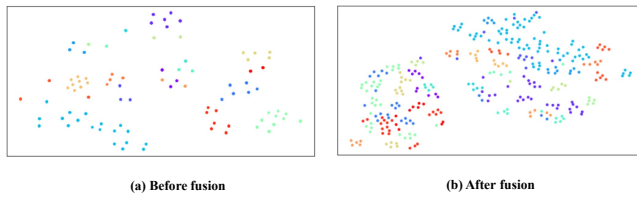


Figure 7: T-SNE for unmixing visualization: on the test split of the multi-source set, the original audio queries A_0 and fused A_6 is visualized. PCA is first applied to divide the audio queries into $K_0 = 20$ clusters, followed by t-sne. More points are depicted after fusion, and audio queries sharing the same color consists of more but closely connect clusters, indicating an unmixed and more informative form.

that AUSS is a promising model for bridging the gap between audio signals and pixel-wise visual semantics.

REFERENCES

- [1] Jimmy Lei Ba, Jamie Ryan Kiros, and Geoffrey E Hinton. 2016. Layer normalization. *arXiv preprint arXiv:1607.06450* (2016).
- [2] Honglie Chen, Weidi Xie, Triantafyllos Afouras, Arsha Nagrani, Andrea Vedaldi, and Andrew Zisserman. 2021. Localizing visual sounds the hard way. In *Proceedings of the IEEE/CVF Conference on Computer Vision and Pattern Recognition*. 16867–16876.
- [3] Liang-Chieh Chen, George Papandreou, Iasonas Kokkinos, Kevin Murphy, and Alan L Yuille. 2017. Deeplab: Semantic image segmentation with deep convolutional nets, atrous convolution, and fully connected crfs. *IEEE transactions on pattern analysis and machine intelligence* 40, 4 (2017), 834–848.
- [4] Liang-Chieh Chen, George Papandreou, Florian Schroff, and Hartwig Adam. 2017. Rethinking atrous convolution for semantic image segmentation. *arXiv preprint arXiv:1706.05587* (2017).
- [5] Bowen Cheng, Ishan Misra, Alexander G. Schwing, Alexander Kirillov, and Rohit Girdhar. 2022. Masked-attention Mask Transformer for Universal Image Segmentation. *CVPR*.
- [6] Bowen Cheng, Alex Schwing, and Alexander Kirillov. 2021. Per-pixel classification is not all you need for semantic segmentation. *Advances in Neural Information Processing Systems* 34 (2021), 17864–17875.
- [7] MMSegmentation Contributors. 2020. MMSegmentation: Openmmlab semantic segmentation toolbox and benchmark.
- [8] Alexey Dosovitskiy, Lucas Beyer, Alexander Kolesnikov, Dirk Weissenborn, Xiuhua Zhai, Thomas Unterthiner, Mostafa Dehghani, Matthias Minderer, Georg Heigold, Sylvain Gelly, et al. 2020. An image is worth 16x16 words: Transformers for image recognition at scale. *arXiv preprint arXiv:2010.11929* (2020).
- [9] Bin Duan, Hao Tang, Wei Wang, Ziliang Zong, Guowei Yang, and Yan Yan. 2021. Audio-visual event localization via recursive fusion by joint co-attention. In *Proceedings of the IEEE/CVF Winter Conference on Applications of Computer Vision*. 4013–4022.
- [10] Brendan Duke, Abdalla Ahmed, Christian Wolf, Parham Aarabi, and Graham W Taylor. 2021. Sstvos: Sparse spatiotemporal transformers for video object segmentation. In *Proceedings of the IEEE/CVF Conference on Computer Vision and Pattern Recognition*. 5912–5921.
- [11] Mark Everingham, Luc Van Gool, Christopher KI Williams, John Winn, and Andrew Zisserman. 2010. The pascal visual object classes (voc) challenge. *International journal of computer vision* 88 (2010), 303–338.
- [12] PK Garg. 2020. Effect of contamination and adjacency factors on snow using spectroradiometer and hyperspectral images. In *Hyperspectral remote sensing*. Elsevier, 167–196.
- [13] Jort F. Gemmeke, Daniel P. W. Ellis, Dylan Freedman, Aren Jansen, Wade Lawrence, R. Channing Moore, Manoj Plakal, and Marvin Ritter. 2017. Audio Set: An ontology and human-labeled dataset for audio events. In *2017 IEEE International Conference on Acoustics, Speech and Signal Processing (ICASSP)*. 776–780. <https://doi.org/10.1109/ICASSP.2017.7952261>
- [14] Kaiming He, Xiangyu Zhang, Shaoqing Ren, and Jian Sun. 2016. Deep residual learning for image recognition. In *Proceedings of the IEEE conference on computer vision and pattern recognition*. 770–778.
- [15] Shawn Hershey, Sourish Chaudhuri, Daniel PW Ellis, Jort F Gemmeke, Aren Jansen, R Channing Moore, Manoj Plakal, Devin Platt, Rif A Saurous, Bryan Seybold, et al. 2017. CNN architectures for large-scale audio classification. In *2017 IEEE international conference on acoustics, speech and signal processing (icassp)*. IEEE, 131–135.
- [16] Yang Jiao, Zequn Jie, Weixin Luo, Jingjing Chen, Yu-Gang Jiang, Xiaolin Wei, and Lin Ma. 2021. Two-stage visual cues enhancement network for referring image segmentation. In *Proceedings of the 29th ACM International Conference on Multimedia*. 1331–1340.
- [17] Alexander Kirillov, Eric Mintun, Nikhila Ravi, Hanzi Mao, Chloe Rolland, Laura Gustafson, Tete Xiao, Spencer Whitehead, Alexander C Berg, Wan-Yen Lo, et al. 2023. Segment anything. *arXiv preprint arXiv:2304.02643* (2023).
- [18] Scott Konishi and Alan L Yuille. 2000. Statistical cues for domain specific image segmentation with performance analysis. In *Proceedings IEEE Conference on Computer Vision and Pattern Recognition. CVPR 2000 (Cat. No. PR00662)*, Vol. 1. IEEE, 125–132.
- [19] Bruno Korbar, Du Tran, and Lorenzo Torresani. 2018. Cooperative learning of audio and video models from self-supervised synchronization. *Advances in Neural Information Processing Systems* 31 (2018).
- [20] Tsung-Yi Lin, Priya Goyal, Ross Girshick, Kaiming He, and Piotr Dollár. 2017. Focal loss for dense object detection. In *Proceedings of the IEEE international conference on computer vision*. 2980–2988.
- [21] Yan-Bo Lin, Yu-Jhe Li, and Yu-Chiang Frank Wang. 2019. Dual-modality seq2seq network for audio-visual event localization. In *ICASSP 2019-2019 IEEE International Conference on Acoustics, Speech and Signal Processing (ICASSP)*. IEEE, 2002–2006.
- [22] Yan-Bo Lin, Hung-Yu Tseng, Hsin-Ying Lee, Yen-Yu Lin, and Ming-Hsuan Yang. 2021. Exploring cross-video and cross-modality signals for weakly-supervised audio-visual video parsing. *Advances in Neural Information Processing Systems* 34 (2021), 11449–11461.
- [23] Yan-Bo Lin and Yu-Chiang Frank Wang. 2020. Audiovisual transformer with instance attention for audio-visual event localization. In *Proceedings of the Asian Conference on Computer Vision*.
- [24] Ze Liu, Yutong Lin, Yue Cao, Han Hu, Yixuan Wei, Zheng Zhang, Stephen Lin, and Baining Guo. 2021. Swin transformer: Hierarchical vision transformer using shifted windows. In *Proceedings of the IEEE/CVF international conference on computer vision*. 10012–10022.
- [25] Ilya Loshchilov and Frank Hutter. 2017. Decoupled weight decay regularization. *arXiv preprint arXiv:1711.05101* (2017).
- [26] Sabarinath Mahadevan, Ali Athar, Aljoša Ošep, Sebastian Hennen, Laura Leal-Taixé, and Bastian Leibe. 2020. Making a case for 3d convolutions for object segmentation in videos. *arXiv preprint arXiv:2008.11516* (2020).
- [27] Yuxin Mao, Jing Zhang, Zhexiong Wan, Yuchao Dai, Aixuan Li, Yunqiu Lv, Xinyu Tian, Deng-Ping Fan, and Nick Barnes. 2021. Transformer transforms salient object detection and camouflaged object detection. *arXiv preprint arXiv:2104.10127* (2021).
- [28] Fausto Milletari, Nassir Navab, and Seyed-Ahmad Ahmadi. 2016. V-net: Fully convolutional neural networks for volumetric medical image segmentation. In *2016 fourth international conference on 3D vision (3DV)*. Ieee, 565–571.
- [29] Rui Qian, Di Hu, Heinrich Dinkel, Mengyue Wu, Ning Xu, and Weiyao Lin. 2020. Multiple sound sources localization from coarse to fine. In *Computer Vision–ECCV 2020: 16th European Conference, Glasgow, UK, August 23–28, 2020, Proceedings, Part XX 16*. Springer, 292–308.
- [30] Olga Russakovsky, Jia Deng, Hao Su, Jonathan Krause, Sanjeev Satheesh, Sean Ma, Zhiheng Huang, Andrej Karpathy, Aditya Khosla, Michael Bernstein, et al. 2015. Imagenet large scale visual recognition challenge. *International journal of computer vision* 115 (2015), 211–252.
- [31] Lukas Schneider, Manuel Jasch, Björn Fröhlich, Thomas Weber, Uwe Franke, Marc Pollefeys, and Matthias Ratsch. 2017. Multimodal neural networks: RGB-D for semantic segmentation and object detection. In *Image Analysis: 20th Scandinavian Conference, SCIA 2017, Tromsø, Norway, June 12–14, 2017, Proceedings, Part I 20*. Springer, 98–109.
- [32] Bowen Shi, Dongsheng Jiang, Xiaopeng Zhang, Han Li, Wenrui Dai, Junni Zou, Hongkai Xiong, and Qi Tian. 2022. A Transformer-Based Decoder for Semantic Segmentation with Multi-level Context Mining. In *European Conference on Computer Vision*. Springer, 624–639.
- [33] Robin Strudel, Ricardo Garcia, Ivan Laptev, and Cordelia Schmid. 2021. Segmenter: Transformer for semantic segmentation. In *Proceedings of the IEEE/CVF international conference on computer vision*. 7262–7272.
- [34] Yapeng Tian, Dingzeyu Li, and Chenliang Xu. 2020. Unified multisensory perception: Weakly-supervised audio-visual video parsing. In *Computer Vision–ECCV 2020: 16th European Conference, Glasgow, UK, August 23–28, 2020, Proceedings, Part III 16*. Springer, 436–454.
- [35] Yapeng Tian, Jing Shi, Bochen Li, Zhiyao Duan, and Chenliang Xu. 2018. Audio-visual event localization in unconstrained videos. In *Proceedings of the European Conference on Computer Vision (ECCV)*. 247–263.
- [36] Laurens Van der Maaten and Geoffrey Hinton. 2008. Visualizing data using t-SNE. *Journal of machine learning research* 9, 11 (2008).
- [37] Ashish Vaswani, Noam Shazeer, Niki Parmar, Jakob Uszkoreit, Llion Jones, Aidan N Gomez, Łukasz Kaiser, and Illia Polosukhin. 2017. Attention is all you need. *Advances in neural information processing systems* 30 (2017).
- [38] Yu Wu and Yi Yang. 2021. Exploring heterogeneous clues for weakly-supervised audio-visual video parsing. In *Proceedings of the IEEE/CVF Conference on Computer Vision and Pattern Recognition*. 1326–1335.
- [39] Yu Wu, Linchao Zhu, Yan Yan, and Yi Yang. 2019. Dual attention matching for audio-visual event localization. In *Proceedings of the IEEE/CVF international conference on computer vision*. 6292–6300.
- [40] Yan Xia and Zhou Zhao. 2022. Cross-modal background suppression for audio-visual event localization. In *Proceedings of the IEEE/CVF Conference on Computer Vision and Pattern Recognition*. 19989–19998.
- [41] Haoming Xu, Runhao Zeng, Qingyao Wu, Mingkui Tan, and Chuang Gan. 2020. Cross-modal relation-aware networks for audio-visual event localization. In *Proceedings of the 28th ACM International Conference on Multimedia*. 3893–3901.
- [42] Hanyu Xuan, Zhenyu Zhang, Shuo Chen, Jian Yang, and Yan Yan. 2020. Cross-modal attention network for temporal inconsistent audio-visual event localization. In *Proceedings of the AAAI Conference on Artificial Intelligence*, Vol. 34. 279–286.
- [43] Jiashuo Yu, Ying Cheng, Rui-Wei Zhao, Rui Feng, and Yuejie Zhang. 2022. Mm-pyramid: Multimodal pyramid attentional network for audio-visual event localization and video parsing. In *Proceedings of the 30th ACM International Conference on Multimedia*. 6241–6249.
- [44] Qihang Yu, Huiyu Wang, Siyuan Qiao, Maxwell Collins, Yukun Zhu, Hartwig Adam, Alan Yuille, and Liang-Chieh Chen. 2022. k-means Mask Transformer. In *Computer Vision–ECCV 2022: 17th European Conference, Tel Aviv, Israel, October 23–27, 2022, Proceedings, Part XXIX*. Springer, 288–307.
- [45] Jing Zhang, Jianwen Xie, Nick Barnes, and Ping Li. 2021. Learning generative vision transformer with energy-based latent space for saliency prediction. *Advances in Neural Information Processing Systems* 34 (2021), 15448–15463.

- [46] Hengshuang Zhao, Jianping Shi, Xiaojuan Qi, Xiaogang Wang, and Jiaya Jia. 2017. Pyramid scene parsing network. In *Proceedings of the IEEE conference on computer vision and pattern recognition*. 2881–2890.
- [47] Hengshuang Zhao, Jianping Shi, Xiaojuan Qi, Xiaogang Wang, and Jiaya Jia. 2017. Pyramid scene parsing network. In *Proceedings of the IEEE conference on computer vision and pattern recognition*. 2881–2890.
- [48] Sixiao Zheng, Jiachen Lu, Hengshuang Zhao, Xiatian Zhu, Zekun Luo, Yabiao Wang, Yanwei Fu, Jianfeng Feng, Tao Xiang, Philip HS Torr, et al. 2021. Rethinking semantic segmentation from a sequence-to-sequence perspective with transformers. In *Proceedings of the IEEE/CVF conference on computer vision and pattern recognition*. 6881–6890.
- [49] Jinxing Zhou, Jianyuan Wang, Jiayi Zhang, Weixuan Sun, Jing Zhang, Stan Birchfield, Dan Guo, Lingpeng Kong, Meng Wang, and Yiran Zhong. 2022. Audio-Visual Segmentation. In *Computer Vision–ECCV 2022: 17th European Conference, Tel Aviv, Israel, October 23–27, 2022, Proceedings, Part XXXVII*. Springer, 386–403.
- [50] Jinxing Zhou, Liang Zheng, Yiran Zhong, Shijie Hao, and Meng Wang. 2021. Positive sample propagation along the audio-visual event line. In *Proceedings of the IEEE/CVF Conference on Computer Vision and Pattern Recognition*. 8436–8444.
- [51] Jinxing Zhou, Liang Zheng, Yiran Zhong, Shijie Hao, and Meng Wang. 2021. Positive sample propagation along the audio-visual event line. In *Proceedings of the IEEE/CVF Conference on Computer Vision and Pattern Recognition*. 8436–8444.

Received 4 May 2023